J Mater Sci (2011) 46:7335–7343
DOI 10.1007/s10853-011-5695-1

Improving bioactivity and durability of yttria-stabilized zirconia

Miho Nakamura · Masahiro Inuzuka · Kazuaki Hashimoto · Akiko Nagai · Kimihiro Yamashita

Received: 13 April 2011 / Accepted: 4 June 2011 / Published online: 16 June 2011

Abstract Because of its excellent mechanical properties, yttria-stabilized zirconia is currently used as an orthopedic and dental material. In this study, we have improved the bioactivity of yttria-stabilized zirconia by a combination of electrical polarization and chemical treatment. The phase transformation from tetragonal to monoclinic ZrO_2 after alkaline treatment was inhibited on positively charged yttria-stabilized zirconia surfaces compared with negatively charged and conventional surfaces. During polarization, some oxide ions move from the positively charged surface to the negatively charged surface, leading to an increase in oxygen vacancies on the positive surface and hence greater formation of Zr–OH when this surface was exposed to alkaline solution. This then reduced the water adsorption at this surface and consequently reduced the rate of cleavage of Zr–O–Zr bonds. The bioactivity was assessed by immersing the samples in simulated body fluid and evaluating the growth of apatite on the surfaces. The combination of polarization and alkaline treatment increased the bioactivity in vitro.

M. Nakamura (✉) · M. Inuzuka · A. Nagai · K. Yamashita
Institute of Biomaterials and Bioengineering, Tokyo Medical and Dental University, 2-3-10 Kanda-Surugadi, Chiyoda, Tokyo 1010062, Japan
e-mail: miho.bcr@tmd.ac.jp

M. Inuzuka · K. Hashimoto
Department of Life and Environmental Science, Chiba Institute of Technology, 2-17-1 Tsudanuma, Narashino, Chiba 2750016, Japan

Introduction

Numerous biomaterials such as ceramics, polymers, metals, and their composites have been developed for orthopedic and dental implant applications. Since the late 1960s, yttria-stabilized zirconia (YSZ), especially 3 mol% Y_2O_3-doped zirconia, has been shown to be a biomaterial with excellent mechanical properties, and YSZ ceramics are currently used as ball heads in artificial hip joints and post-crowns in dental applications [1–4]. YSZ is, however, bioinert, meaning that no direct bonding of YSZ to natural bones occurs in vivo. In this study, we have addressed this shortcoming by employing chemical treatments with the aim of increasing the bioactivity of YSZ.

We have recently demonstrated that the ceramic hydroxyapatite (HA) [5–7] may be polarized via proton migration [7, 8], and that the polarized surfaces of HA enhanced tissue regeneration of both hard [9, 10] and soft [11, 12] tissues in vivo. Three weeks after implantation into the tibiae of rabbits, new bone formation was accelerated in the center of the polarized porous HA samples compared with conventional porous HA samples [10]. The polarized HA enhanced the blood regeneration of a vascular injury model [11] and epidermal recovery from full-thickness skin wounds in vivo [12]. In addition, the polarized HA also accelerated protein adsorption [13] and cell adhesion through improved wettability of water [14]. Thus, electrical polarization can have excellent chemical, biological, and biomedical effects.

Another serious problem with YSZ lies in its instability due to a tetragonal (t) to monoclinic (m) phase transformation at relatively low temperatures of (<400 °C) in moist air or hot water [15–17]. These phenomena are usually termed low temperature degradation (LTD). Kobayashi et al. [18] have reported that the annealing

treatment of zirconia at 65–400 °C in water for a long time spontaneously gave rise to the transformation of tetragonal into monoclinic phase. This t–m phase transformation in YSZ is reportedly accompanied by cracking on the surface due to the volume expansion of about 4–5% and degradation of mechanical strength [19], which can cause critical accidents in medical applications.

Although LTD has been thoroughly demonstrated, the exact mechanism is not fully understood [20, 21]. Sato et al. [15] proposed that the chemisorbed water molecules form Zr–OH at the surface, resulting in the release of strain energy that would ensue if the t–m transformation was to occur. Yoshimura suggested that the accumulated strain region resulting from the migration of hydroxide ions at the surface and in the lattice serves as a nucleus of the monoclinic ZrO_2 phase in the tetragonal ZrO_2 matrix [22]. Recently, the use of higher valency metal ions such as Nb^{5+} and Ce^{4+} has been proven to be effective for suppression of LTD because the oxygen vacancies decrease with the substitution [23–27]. Djurado et al. [28] believed that no Zr or Y hydroxides interact in the t–m transformation mechanism of YSZ due to the absence of the hydroxide ion signature in the Raman spectra, either on the surface or in the volume.

It is crucial to inhibit the LTD of YSZ in medical and structural applications and also to understand the role of moisture in LTD. We observed that our polarization process successfully inhibited LTD in the chemical treatments of YSZ ceramics. This report details the bioactivation and LTD-inhibition of polarized YSZ ceramics and discusses the polarization mechanisms.

Materials and methods

Preparation, characterization, and electrical properties of YSZ samples

Yttria partially stabilized zirconia powder (TZ-3Y, Tosoh, Japan) was pressed into a mold at 120 MPa. The YSZ compacts were sintered in air at 1400 °C for 1 h. The relative density values of the sintered YSZ compacts were ca. 99.2 ± 0.1%.

Impedance measurements were carried out in air using an impedance analyzer (16048A Hewlett Packard) over a frequency range of 100 Hz–1 MHz. A four-probe a.c. method with platinum ion blocking electrodes and attached platinum wires was used to measure the complex conductivity. The resistance (R) of the samples was determined from the obtained Cole–Cole plots. For a given geometry, the ion conductivity (σ) at each temperature and the Arrhenius plots for the YSZ ceramics were calculated.

Electrical polarization and thermally stimulated depolarization current measurement

The sintered YSZ samples were electrically polarized as previously described [7] with a pair of platinum electrodes at 200 °C in a direct-current (d.c.) electric field of 20 V cm^{-1} for 30 min in air. Polarization of the YSZ samples was verified by thermally stimulated depolarization current (TSDC) measurements. The TSDC measurements were carried out in air from room temperature (RT) to 600 °C at a heating rate of 5.0°C min^{-1} also as previously described [7]. The depolarization current was measured with a Hewlett-Packard 4140B pA meter. The values of the polarization charge (Q_p) were calculated from the TSDC spectra using the equation

$$Q_p = \frac{1}{\beta}\int J(T)\mathrm{d}T \quad (1)$$

where $J(T)$ is the measured dissipation current density at temperature, T and β is the heating rate.

Preparation and characterization of chemically treated YSZ samples

The electrically polarized YSZ samples were treated with either alkaline (5 mol dm^{-3} NaOH at 95 °C for 24 h) or with acidic (5 mol dm^{-3} H_3PO_4 at 95 °C for 24 h) solutions in commercial glass tubes. After chemical treatment, the samples were washed with deionized water and dried at 60 °C for 3 h.

X-ray diffraction (XRD) measurements for phase analysis of the chemically treated YSZ surfaces were performed at room temperature with Cu–Kα radiation at 40 kV and 40 mA on a Philips PW 1700 diffractometer equipped with a graphite monochromator. The extents of phase transformation of the chemically treated YSZ samples were calculated using the equation of Garvie and Nicholson [29]

$$X_m(\mathrm{mol}\%) = \frac{I_m(111) + I_m(11\bar{1})}{I_m(111) + I_m(11\bar{1}) + I_t(111)} \times 100 \quad (2)$$

where I is the integral intensity, m is monoclinic, and t is tetragonal.

Compositional analysis was carried out using X-ray photoelectron spectroscopy (XPS) on a JPS-90SX spectrometer (Japan) with Al Kα X-rays at an analytical angle of 45°. The C 1 s peak was used for calibration of the binding energies by setting its binding energy to 284.6 eV to correct for sample charging.

SBF immersion test

The YSZ samples were immersed in simulated body fluid (SBF) with pH 7.4 at 37 °C for 4 and 6 days. SBF solution

was prepared using the technique described by Kokubo et al. [30, 31]. After immersion in SBF, the samples were washed with deionized water and ethanol, and then dried at *RT* in air. The surfaces were sputtered with Pt–Pd using an ion coater (Eiko Engineering IB-2). The sputtered surfaces were observed using a scanning electron microscope (SEM, Hitachi S-2400).

Statistical analysis

Accurate quantification in different films was achieved by three independent experiments. The differences between the two groups were analyzed using one- or two-way analysis of variance (ANOVA). Student's *t* test (paired or unpaired) was used to ascertain the differences between the two groups. Statistical significance was defined as $P < 0.05$.

Results and discussion

Impedance measurement

YSZ is known as a high temperature O^{2-} conductor, however, the temperature used for our polarization experiments is around 200 °C. Typical complex-impedance plots of YSZ at temperatures from 190 to 400 °C are shown in Fig. 1, where the calculated values of σ represent the conductivities of grains and grain boundaries, since the diagrams contain two semicircles. The semicircles at higher frequencies were detected at temperatures from 100 to 400 °C and attributed to the impedance of the grains, while the semicircles at lower frequencies were detected at higher temperatures from 240 to 600 °C, and are attributed to the impedance of grain boundaries [32, 33]. The calculated conductivity displays Arrhenius behavior, with the activation energy of conduction being 71 kJ mol^{-1} for the grains and 83 kJ mol^{-1} for the grain boundaries. The plot shows that the resistances of grains and grain boundaries are comparable at the polarization temperature of 200 °C. This is important, since it indicates that the external d.c. voltage was equally applied to grains and grain boundaries.

TSDC measurement

The TSDC spectra of as-polarized YSZ increased at ca. 200 °C, had two peaks at ca. 300 and 420 °C and then gradually decreased (Fig. 2). The TSDC measurement of the d.c. electrically treated YSZ demonstrates that the YSZ is actually polarized with a significant stored energy of 2.0 mC cm^{-2}, obtained according to Eq. 1. The activation energy for depolarization calculated from the TSDC spectra according to the Arrhenius formula was 0.76 eV for as-polarized YSZ, similar to the activation energy for O^{2-} conduction through grains. This supports the hypothesis that polarization takes place due to O^{2-} migration through the applied d.c. field.

The possible influence of chemical treatment on the polarization of YSZ was evaluated by comparing the TSDC spectra of chemically treated YSZ with that of as-polarized YSZ. The TSDC curves shows that the chemical treatments in both alkaline and acid solutions have no influence on the polarization of YSZ (Fig. 2). All of the TSDC curves increased at ca. 200 °C, reached maxima at ca. 300 °C, and then gradually decreased. The stored charges (Q) from the TSDC spectra were calculated at 2.01 mC cm^{-2} for as-polarized YSZ, 2.00 mC cm^{-2} for YSZ after the alkaline treatment and 1.52 mC cm^{-2} for YSZ after the acidic treatment.

On the basis of the impedance and TSDC results, there are two mechanisms involved in YSZ depolarization: depolarization in grains occurs below about 300 °C and depolarization around grain boundaries occurs above 300 °C. Partial stabilization of yttria in the zirconia structure forms oxygen vacancies, which act as the ionic migration path during polarization [34]. Oxide ions were forced to move toward the side of YSZ-N during polarization, which consequently induced an increase in oxygen vacancy content on the YSZ-P side.

XRD and XPS after chemical treatment

The XRD patterns of the normal YSZ (YSZ-O), negatively charged YSZ (YSZ-N), and positively charged YSZ (YSZ-P) were highly consistent with the published data for ZrO_2 (ICDD no. 79-1796), indicating that the YSZ surfaces consisted of a single phase of tetragonal ZrO_2 before and after electrical polarization (Fig. 3A). As shown in Fig. 3B, the XRD patterns for the YSZ-O, YSZ-N, and YSZ-P after alkaline treatment consisted of the phases of tetragonal ZrO_2 and monoclinic ZrO_2 (ICDD no. 37-1484). The extents of the phase transformation from tetragonal ZrO_2 to monoclinic ZrO_2 after alkaline treatment were 9.6, 10.4, and 1.5 mol %, for YSZ-O, YSZ-N, and YSZ-P, respectively (Fig. 3D). The phase transformation was significantly inhibited on the YSZ-P surface. The XRD patterns of the YSZ-O, YSZ-N, and YSZ-P after acidic treatment consisted of the phases of tetragonal ZrO_2 and monoclinic ZrO_2 (Fig. 3C). The extents of the phase transformation from tetragonal ZrO_2 to monoclinic ZrO_2 after acidic treatment were 12.4, 11.8, and 10.5 mol% for YSZ-O, YSZ-N, and YSZ-P, respectively (Fig. 3E). Thus, alkaline treatment promotes t → m transformation on each surface of YSZ-O, YSZ-N, and YSZ-P, while the polarized YSZ-P surface was proven to be remarkably resistant to LTD in alkaline solution.

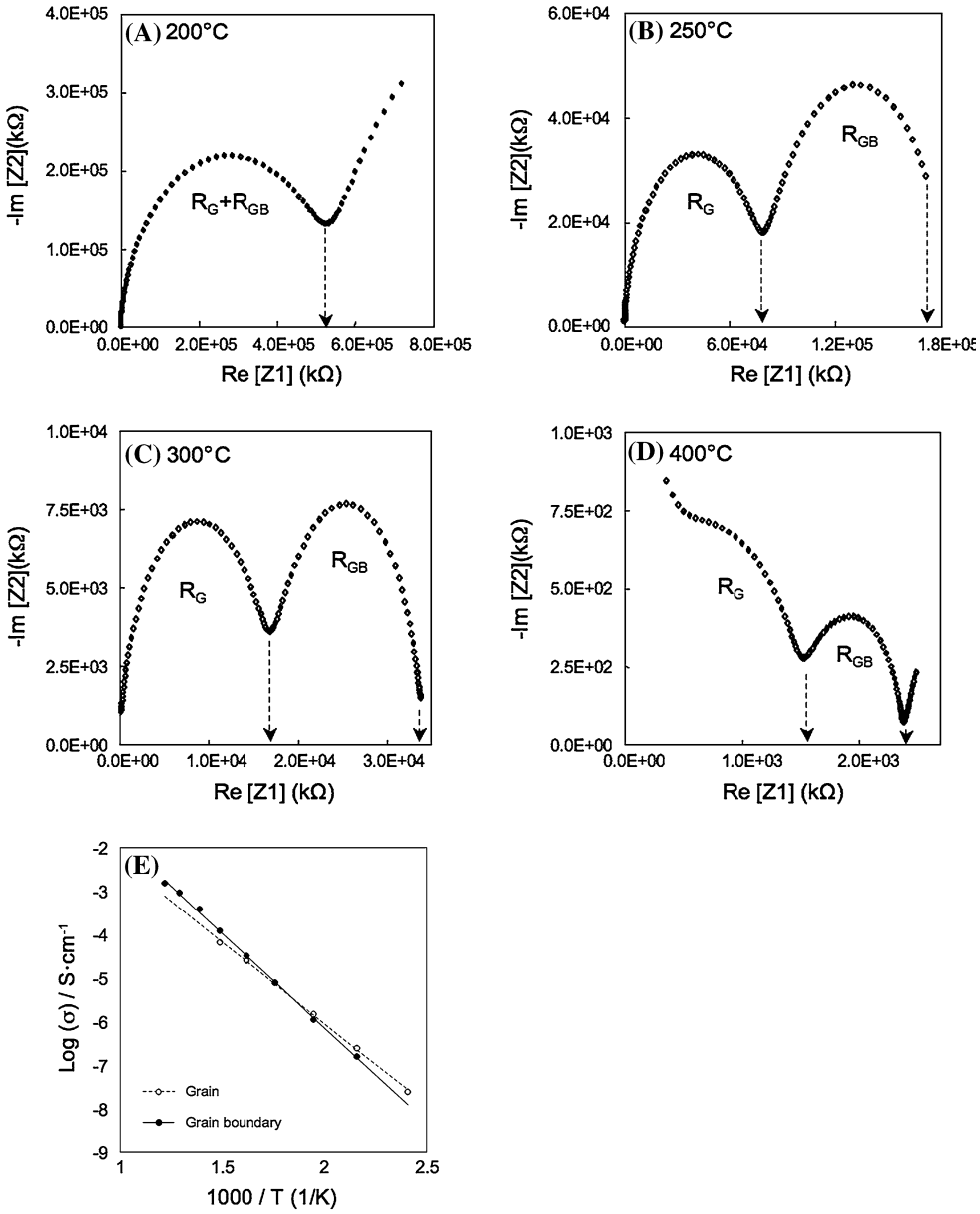

Fig. 1 Typical complex-impedance diagrams of YSZ at **A** 200 °C, **B** 250 °C, **C** 300 °C, and **D** 400 °C. **E** Arrhenius plots of YSZ ceramics calculated from Cole–Cole plots of complex-impedance measurements

Figure 4 shows the detailed XPS scans for oxygen 1 s of YSZ-O, YSZ-N, and YSZ-P after the chemical treatments. The peak in binding energies of oxygen appeared for the alkaline-treated surfaces from 530 to 532 eV, which was decomposed into two peaks: 532 eV for H_2O or OH groups and 530 eV for ZrO_2 [35]. The ratios of the areas of H_2O or OH group to total oxygen in YSZ-O, YSZ-N, and YSZ-P were 36.2, 36.1, and 55.7%, respectively (Fig. 4C). More hydroxyl groups were formed on the YSZ-P surface, compared with the YSZ-O and YSZ-N. As shown in Fig. 4B, the peak for binding energies of oxygen appeared on the acidic treated surfaces from 530 to 532 eV, and was also decomposed into two peaks: 532 eV for H_2O or OH groups and 530 eV for ZrO_2. The ratios of the areas of H_2O or OH groups to oxygen areas in YSZ-O, YSZ-N, and YSZ-P were 47.3, 52.7, and 61.2%, respectively (Fig. 4D). As with the alkaline treatment, more hydroxyl groups were formed on the YSZ-P surface, compared with the YSZ-O and YSZ-N. In general, the amount of hydroxyl groups was greater on the acidic treated surfaces than on the alkaline-treated surfaces.

Sato et al. [36] concluded that the phase transformation resulted from Zr–OH formation from chemical reactions between ZrO_2 and H_2O on the YSZ surfaces instead of the release of zirconium and yttrium ions even in corrosive solutions at 95 °C. The mechanism of Zr–OH formation on the YSZ surface was reported to progress in three stages: (1) the formation of hydrogen bonds between the protons of water molecules and the oxygen atoms of Zr; (2) two concerted coupling reactions: one between the proton of

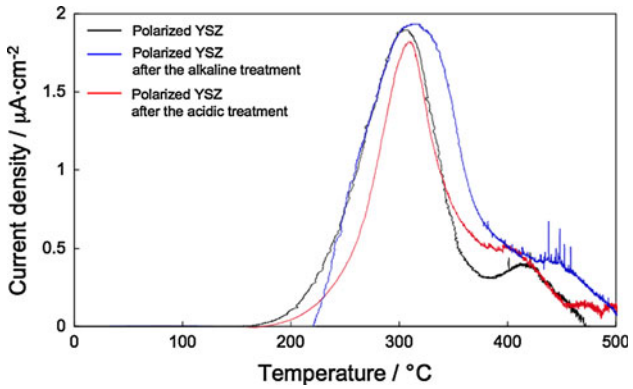

Fig. 2 TSDC spectra of the as-polarized YSZ, the polarized YSZ after alkaline treatment, and the polarized YSZ after acidic treatment. All of the TSDC curves increased at ca. 200 °C, reached maxima at ca. 300 °C, and then gradually decreased. The stored charge values (*Q*) from the TSDC spectra were calculated as 2.01 mC cm^{-2} for as-polarized YSZ, 2.00 mC cm^{-2} for YSZ after alkaline treatment and 1.52 mC cm^{-2} for YSZ after acidic treatment

water molecules and the oxygen atom of Zr and a second between the oxide ions of water molecules and the Zr atoms; (3) the cleavage of the Zr–O-Zr bonds and the formation of Zr–OH by the phase transformation [36–38]. During the phase transformation, both the binding forces and the strain energies were decreased due to microcrack formation by the cleavage of Zr–O–Zr bonds [36, 39].

SBF immersion test after chemical treatment

The surfaces of YSZ-O, YSZ-N, and YSZ-P after SBF immersion for 6 days had no significant differences as shown in Fig. 5. Deposits of bone-like apatite crystals had formed and grown to ca. 1 μm in diameter on the alkaline-treated YSZ-P after immersion for 4 days, whereas there were no deposits on the alkaline-treated YSZ-O and YSZ-N surfaces. After the immersion for 6 days, deposits of bone-like apatite crystals were also observed on the alkaline-treated YSZ-O and YSZ-N surfaces (data not shown). The deposits of bone-like apatite crystals were also observed on the surfaces of the acidic-treated YSZ-O, YSZ-N, and YSZ-P after SBF immersion for 4 days, which indicated that there are no obvious differences between different polarizations of YSZ surfaces after the acidic treatment.

The YSZ surfaces after chemical treatment in both alkaline and acidic solutions showed the phase transformation from tetragonal ZrO_2 to monoclinic ZrO_2 and the deposition of bone-like apatite crystals after immersion in SBF. These results, when combined with the mechanism proposed by Sato et al. [36], suggest that the Zr–OH

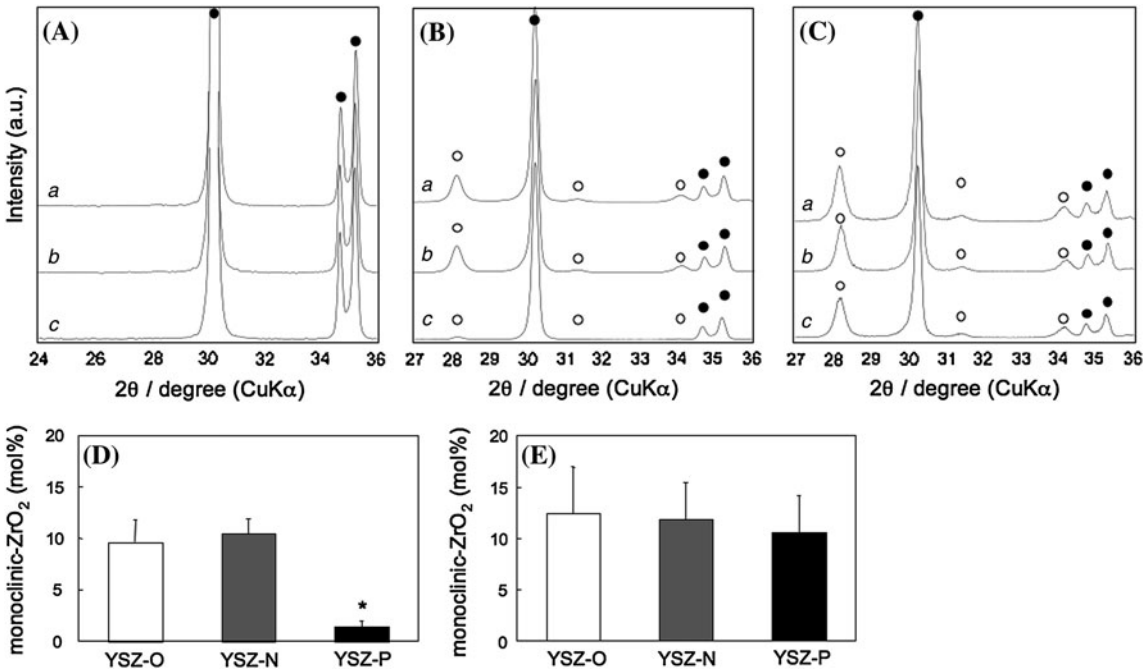

Fig. 3 **A** XRD patterns of *a* YSZ-O, *b* YSZ-N, and *c* YSZ-P. All surfaces were highly consistent with tetragonal ZrO_2 (*closed circles*), indicating that the as-polarized YSZ surfaces consisted of a single phase of tetragonal ZrO_2 before and after electrical polarization. **B** XRD patterns of YSZ samples after the alkaline treatment. All surfaces consisted of both tetragonal ZrO_2 (*closed circles*) and monoclinic ZrO_2 (*open circles*) phases. **C** XRD patterns of YSZ samples after acidic treatment. All surfaces consisted of both tetragonal ZrO_2 (*closed circles*) and monoclinic ZrO_2 (*open circles*) phases. **D** Extent of phase transformation from tetragonal ZrO_2 into monoclinic ZrO_2 after alkaline treatment. (* < 0.001) **E** Extent of phase transformation from tetragonal ZrO_2 into monoclinic ZrO_2 after acidic treatment

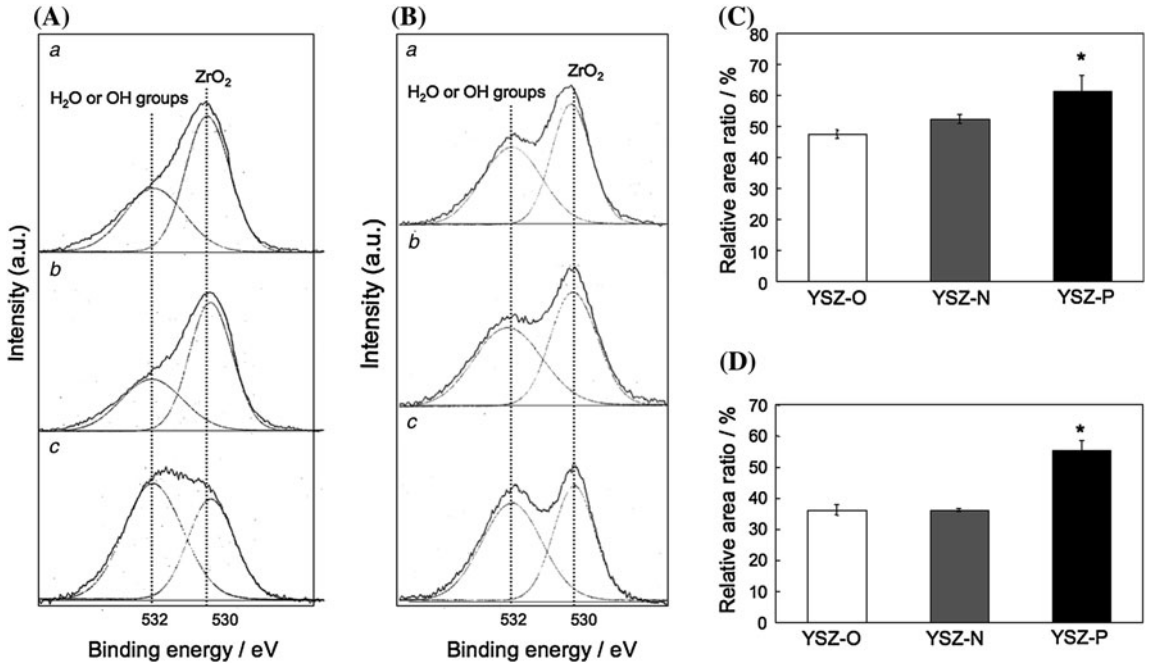

Fig. 4 **A** Detailed XPS scans for oxygen 1 s of *a* YSZ-O, *b* YSZ-N, and *c* YSZ-P after alkaline treatment. **B** Detailed XPS scans for oxygen 1 s of *a* YSZ-O, *b* YSZ-N, and *c* YSZ-P after acidic treatment. **C** Ratios of the areas of H_2O or OH groups to oxygen in YSZ samples after alkaline treatment. ($* < 0.01$) **D** Ratios of the areas of H_2O or OH groups to oxygen in YSZ samples after acidic treatment. ($* < 0.02$)

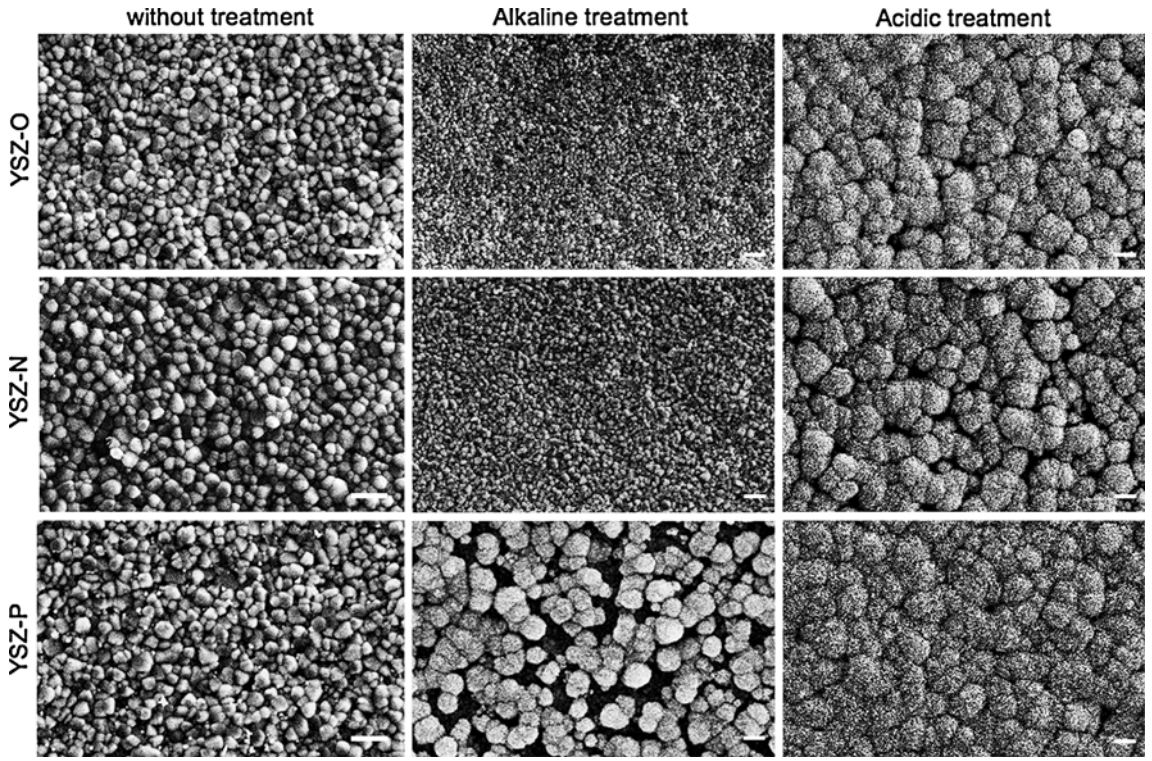

Fig. 5 SEM images of the surfaces of YSZ samples after SBF immersion. There were no significant differences among the surfaces of YSZ-O, YSZ-N, and YSZ-P without any chemical treatment after SBF immersion for 6 days. Deposition of bone-like apatite crystals of around 1 μm in diameter was observed on the alkaline-treated YSZ-P after immersion for 4 days, whereas there were no deposits on the alkaline-treated YSZ-O and YSZ-N surfaces after similar immersion. Deposition of bone-like apatite crystals was also observed on the surfaces of the acidic-treated YSZ-O, YSZ-N, and YSZ-P after SBF immersion for 4 days, which indicated that there are no obvious differences between the YSZ surfaces after acidic treatment. (*Bar* 1 μm)

formed on the YSZ surfaces by the chemical treatment induced the nucleus formation of apatite crystals when the surfaces were immersed in SBF solution. However, although the amount of OH groups was larger on the chemically treated YSZ-P than the chemically treated YSZ-O and YSZ-N, the phase transformation was inhibited on the chemically treated YSZ-P surface. This result is incompatible with the mechanisms proposed by Sato et al. On the other hand, Uchida et al. [31, 40] showed that apatite crystals were deposited on chemically treated Ce–TZP/Al_2O_3 by the formation of Zr–OH without phase transformation. Thus, the Zr–OH formation on our YSZ surfaces must result not only from the aforementioned mechanism proposed by Sato et al. but also from some other mechanism.

Hydroxide ions have been reported to penetrate into the oxygen vacancies on the surface and in the lattice of 2.66 (mol%) yttria partially stabilized zirconia samples sintered at 1450 °C for 2 h after hydrothermal treatment at high pressure, based on the measurement of the lattice constant [22].

$$\mathrm{Zr}_{1-\chi}\mathrm{Y}_{\chi}\mathrm{O}_{2-\chi/2}\square_{\chi/2} + \delta\mathrm{H}_2\mathrm{O} \Leftrightarrow (\mathrm{Zr}_{1-\chi})\ \mathrm{O}_{2-\chi/2-\delta}(\mathrm{OH})_{2\delta}\square_{\chi/2-\delta}$$

where $\chi = 0.0518$ and $\delta = 0.0159$.

Thus, the alkaline treatment induced a reaction on the YSZ-P surface and formed oxygen vacancies (V_O) as described below [37]:

$$\mathrm{Y_2O_3} + 2\mathrm{Zr}_{\mathrm{Zr}}^{\times} + \mathrm{O}_{\mathrm{o}}^{\times} \xrightarrow{\mathrm{ZrO_2}} 2\mathrm{Y}_{\mathrm{Zr}}^{\bullet} + \mathrm{V}_{\mathrm{o}}^{\bullet\bullet} + 2\mathrm{ZrO_2}$$

Since there are oxygen vacancies in the YSZ structure, the likely carrier of polarization in YSZ is oxide ions. During the polarization treatment of YSZ, the oxide ions migrate to the oxygen vacancies near the negatively charged surface induced at the cathode, resulting in an increase in concentration of oxygen vacancies near the positively charged surface induced at the anode.

By the definition of Bronsted–Lowry, water molecules exist as oxonium or hydroxide ions in alkaline solution. Thus, the hydroxide ions are attracted to the oxygen vacancies near the positively charged YSZ surface and may enter these vacancies, inducing the formation of Zr–OH on the YSZ-P:

$$\mathrm{V}_{\mathrm{o}}^{\bullet\bullet} + \mathrm{OH}^{\bullet} \rightarrow \mathrm{OH}_{\mathrm{o}}^{\bullet}$$

The LTD resistance of the YSZ-P was attributed to lower cleavage of Zr–O–Zr bonds via the adsorption of water molecules.

This formation of Zr–OH groups on both the YSZ-O and YSZ-N surfaces was consistent with the results of the extent of phase transformation after the chemical treatment (from XRD) and the equal amount of hydroxyl groups (from XPS). The formation of Zr–OH groups was accelerated on the YSZ-P surface by the selective attraction of hydroxide ions into the oxygen vacancies in comparison with the YSZ-O and YSZ-N surfaces. The Zr–OH groups were considered to contribute to the nucleus formation during the deposition of bone-like apatite crystals from SBF solution (Fig. 6A).

Based on the XPS spectra, the formation of Zr–OH increased on the YSZ surfaces after the acidic treatment. These results are consistent with those reported by Uchida et al. [29, 40]. The mechanisms of Zr–OH formation are, therefore, different in alkaline and acidic solutions.

Water molecules exist as hydroxide ions and protons in an acidic solution. The hydroxide ions were attracted to the YSZ-P surface, while the protons were attracted to the YSZ-N surface. The XPS spectra of the surfaces of YSZ-P, YSZ-N, and YSZ-O showed that the greatest amount of the Zr–OH formed on the YSZ-P surface for this treatment. Therefore, the mechanism of the Zr–OH formation was different between the YSZ-N and YSZ-P surfaces, presumably because the YSZ-N attracted the protons and the YSZ-P attracted the hydroxide ions.

Figure 6B shows the mechanism of Zr–OH formation in acidic solution. The hydrogen bonding between the protons attracted to the YSZ-N surface and the oxide ions of zirconia formed Zr–OH. From the XRD patterns of the YSZ surfaces after acidic treatment, the extent of the phase transformations were almost independent of polarization. The mechanism of the Zr–OH formation is, therefore, different from that induced by the cleavage of Zr—O–Zr bonding reported by Sato et al. [36]. The Zr–OH formation was induced on the YSZ-P surfaces after acidic treatment by the attraction of hydroxide ions and their insertion into the oxygen vacancies, as for YSZ-P subjected to alkaline treatment. The extent of both mechanisms of Zr–OH formation (insertion of hydroxide ions into oxygen vacancies and cleavage of Zr–O–Zr bonds) were decreased on the YSZ-O surface, resulting in only a small amount of the Zr–OH formation on this surface.

Our results for the extent of phase transformation (from XRD) on YSZ-O and YSZ-N agree with the reports by Sato et al. that the alkaline or acidic treatments had no effects on the phase transformation from tetragonal ZrO_2 to monoclinic ZrO_2. Although the alkaline treatment suppressed the phase transformation on the YSZ-P surface, the acidic treatment had no effect on the phase transformation of YSZ-O, YSZ-N, and TSZ-P surfaces. This is probably associated with differences in the release of zirconium ions. Uchida et al. [31] believed that the formation of Zr–OH was greater in the acidic treatment than in the alkaline treatment, because the release of the zirconium ions increased in the acidic solution based on their atomic adsorption spectrochemical analysis. We hypothesize that the zirconium ions are equally released from the YSZ-O,

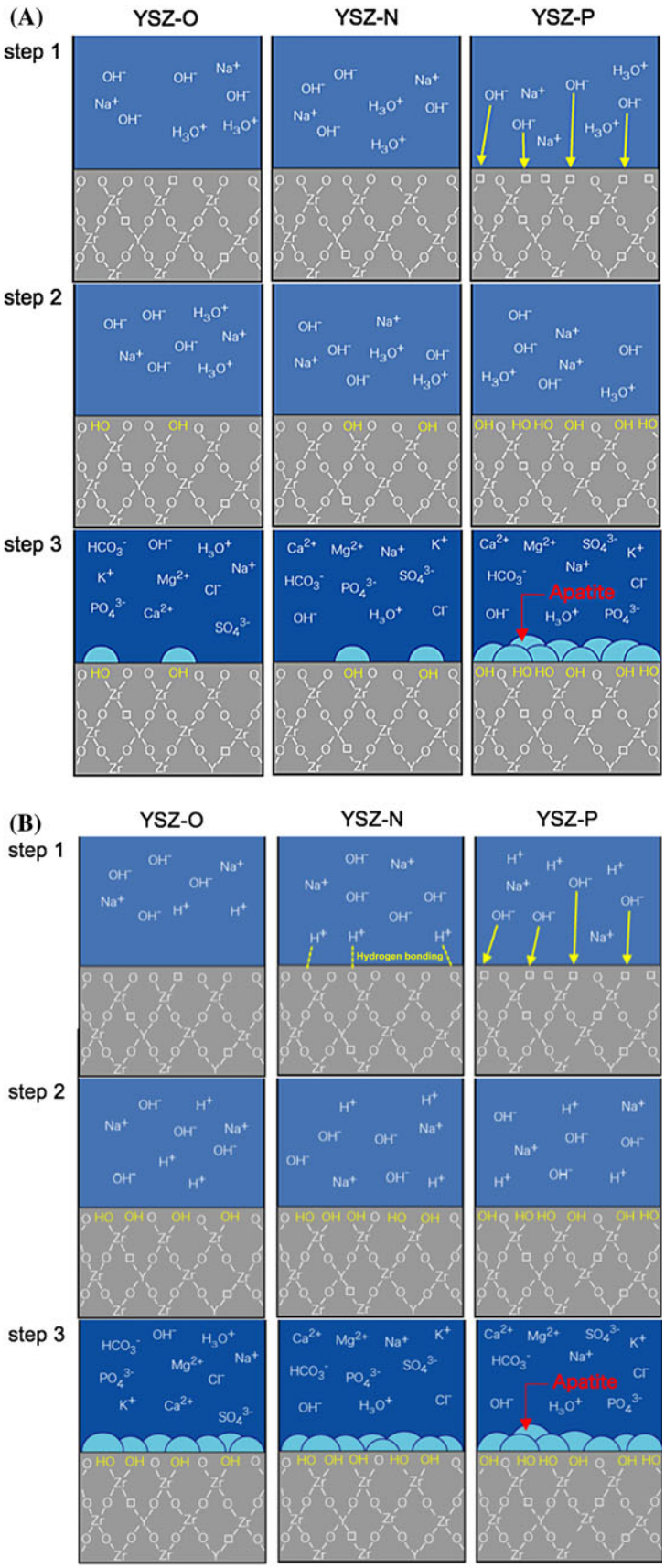

Fig. 6 Illustrations of the proposed model for **A** the formation of Zr–OH functional groups on the alkaline treated YSZ surfaces and **B** the formation of Zr–OH functional groups on the acidic treated YSZ surfaces. **A** Formation mechanism of Zr–OH functional groups on alkaline-treated YSZ-P surface and bone-like apatite-formation mechanism. *Step 1* Hydroxide ions are attracted to oxide vacancies on the YSZ-P surface. *Step 2* Many Zr–OH functional groups are formed on the YSZ-P surface. *Step 3* Apatite formation is initiated by these Zr–OH functional groups on the YSZ-P surface. **B** Formation mechanism of Zr–OH functional groups on acidic-treated YSZ-P surface and bone-like apatite-formation mechanism. *Step 1* Hydrogen ions attracted to the YSZ-N bind to the oxide ions of zirconia. Hydroxide ions are attracted to the oxide vacancies of the YSZ-P surface. *Step 2* Many Zr–OH functional groups are formed on both YSZ-N and YSZ-P surfaces. *Step 3* Apatite formation is induced by these Zr–OH functional groups on the YSZ surfaces

YSZ-N, and YSZ-P surfaces in the acidic solutions, and hence the surfaces have similar phase transformations through this etching effect. The formation of Zr–OH via the release of the zirconium ions is also a possible explanation for the similar depositions of bone-like apatite crystals on the YSZ-O, YSZ-N, and YSZ-P after the acidic treatment.

Conclusions

There are two mechanisms for YSZ depolarization: depolarization in grains at lower temperatures and depolarization at grain boundaries at higher temperatures. The polarization of YSZ samples polarized via these two mechanisms at grain and grain boundaries was maintained during the chemical treatments.

Surface characterization shows that the phase transformation after the alkaline treatment was inhibited on the YSZ-P surface compared with YSZ-N and YSZ-O. This was attributed to a decrease in cleavage of Zr–O–Zr bonds induced by the adsorption of water molecules onto oxide ions on the YSZ-P surface, since this surface has less oxide ions. Among the alkaline-treated samples, the most hydroxyl groups were formed on the surface of YSZ-P. The alkaline treatment formed oxygen vacancies on the YSZ-P surface. Cleavage of Zr–O–Zr bonds lead to microcrack formation and promoted both the phase transformation and Zr–OH formation.

Although the polarization had no effects on the YSZ surfaces after the SBF immersion without any chemical treatment, the combination of the polarization and alkaline treatment induced the depositions of bone-like apatite crystals. This is because the distinct formation of Zr–OH on the YSZ-P acted as the nucleus for formation of apatite crystals in SBF solution.

References

1. Yang Y, Ong JL, Tian J (2003) Biomaterials 24:619
2. Li J, Hastings GW (1998) Handbook of biomaterials properties. Chapman and Hall, New York, p 321
3. Chevalier J, Aza AHD, Fantozzi G, Schehl M, Torrecillas R (2000) Adv Mater 12:1619
4. Chevalier J (2006) Biomaterials 27:535
5. Yamashita K, Oikawa N, Umegaki T (1996) Chem Mater 12:2697
6. Yamashita K, Nakamura S (2005) J Ceram Soc Jpn 113:1
7. Nakamura S, Takeda H, Yamashita K (2001) J Appl Phys 89(10):5386
8. Tanaka Y, Iwasaki T, Nakamura M, Nagai A, Katayama K, Yamashita K (2010) J Appl Phys 107:014107
9. Kobayashi T, Nakamura S, Yamashita K (2001) J Biomed Mater Res 57(4):477
10. Itoh S, Nakamura S, Kobayashi T, Shinomiya K, Yamashita K (2006) Calcified Tissue Int 78(3):133
11. Nagai A, Yamashita K, Imamura M, Azuma H (2008) Life Sci 82(23–24):1162
12. Okabayashi R, Nakamura M, Okabayashi T, Tanaka Y, Nagai A, Yamashita K (2009) J Biomed Mater Res Appl Biomater B 90:641
13. Nakamura M, Nakamura S, Sekijima Y, Niwa K, Kobayashi T, Yamashita K (2006) J Biomed Mater Res A 79(3):627
14. Nakamura M, Nagai A, Hentunen T, Salonen J, Sekijima Y, Okura T, Hashimoto K, Toda Y, Monma H, Yamashita K (2009) ACS Appl Mater Interfaces 1(10):2181
15. Sato T, Ohtaki S, Shimada M (1985) J Mater Sci 20:1466. doi: 10.1007/BF01026344
16. Sato T, Shimada M (1985) J Am Ceram Soc 68:356
17. Chevalier J, Deville S, Munch E, Jullian R, Lair F (2004) Biomaterials 25:5539
18. Kobayashi K, Kuwajima H, Masaki Y (1981) Solid State Ionics 3/4:489
19. Sato T, Ohtaki S, Endo T, Shimada M (1986) J Mater Sci Lett 5:1140
20. Lange FF, Dunlop GL, Davis BI (1986) J Am Ceram Soc 69:237
21. Schmauder S, Schubert H (1986) J Am Ceram Soc 69:534
22. Yohimura M (1988) Am Ceram Soc Bull 67:1950
23. Kim DJ, Jung HJ, Jang JW, Lee HL (1998) J Am Ceram Soc 81:2309
24. Lin JD, Cuh JG, Lo CL (2001) Mater Chem Phys 77:808
25. Tanaka K, Tamura J, Kawanabe K, Nawa M, Uchida M, Kokubo T, Nakamura T (2003) J Biomed Mater Res 67A:200
26. Gutierrez-Gonzalez CF, Moya J, Palomares Bartolome JF (2010) J Am Ceram Soc 93:1842
27. Kim DJ, Lee MH, Lee FY, Han JS (2000) J Biomed Mater Res 53:438
28. Djurado E, Boulc'h F, Dessemond L, Rosman N, Mermoux M (2004) J Electrochem Soc 151:A774
29. Garvir RG, Nicholson PS (1972) J Am Ceram Soc 55:303
30. Kokubo T, Kushitani H, Sakka S, Kitsugi T, Yamamuro T (1990) J Biomed Mater Res 24:721
31. Uchida M, Kim HM, Kokubo T, Nawa M, Asano T, Tanaka K, Nakamura T (2002) J Biomed Mater Res 60:277
32. Bauerle JE (1969) J Phys Chem of Solids 30:2657
33. Lee J, Kim D (2001) J Mater Res 16–9:2739
34. Martin MC, Mecartney ML (2003) Solid State Ionics 161:67
35. Li JF, Watanabe R, Zhanf BP, Asami K, Hashimoto K (1996) J Am Ceram Soc 79:3109
36. Sato T, Fujishiro H, Endo T, Shimada M (1987) J Mater Sci 22:882. doi:10.1007/BF01103525
37. Guo X (2003) J Am Ceram Soc 86:1867
38. Guo X (2004) Chem Mater 16:3988
39. Aza AHD, Chevalier J, Fantozzi G, Schehl M, Torrecillas R (2002) Biomaterials 23:937
40. Uchida M, Kim HM, Miyaji F, Kokubo T, Nakamura T (2002) Biomaterials 23:313